Eur. Phys. J. B (2016) 89: 258
DOI: 10.1140/epjb/e2016-70448-0

THE EUROPEAN PHYSICAL JOURNAL B

Regular Article

Theoretical study of the effect of hydrogen adsorption on the stability and electronic properties of hybrid monolayers

Thiago S. Silva[1], Sérgio Azevedo[1,a], and Bertúlio de Lima Bernardo[2]

[1] Departamento de Física, Universidade Federal da Paraíba, Caixa Postal 5008, 58051-970 João Pessoa, PB, Brazil
[2] Unidade Acadêmica de Física, Universidade Federal de Campina Grande, 58429-140 Campina Grande, PB, Brazil

Received 22 July 2016 / Received in final form 31 August 2016
Published online 28 November 2016 –

Abstract. We have applied first-principle calculations, based on the density functional theory, to analyze the stability, electronic and magnetic properties of monolayers of graphene with a nanodomain of boron nitride (h-BN) with different geometries. To this end, we have investigated the effects of the adsorption of one and two hydrogen atoms by different atoms at the edge of the h-BN nanodomain, where we used the GGA approximation for the functional exchange and correlation. Specifically, we found that the structures with triangular-shaped nanodomains are the most stable and have a non-integer magnetic moment upon adsorption of the hydrogen atoms. We have also shown that both the electronic and magnetic properties can be influenced by the type of atom which adsorbs the hydrogen at the edge of the nanodomain. Additionally, we have demonstrated that some structures can quench the spin that would be generated by the adsorption of the hydrogen atoms.

1 Introduction

In recent years we have witnessed an increasing interest in carbon-based materials [1–3]. Due to the hybridization properties, the carbon atoms are capable of forming various extended structures with diverse electronic, magnetic and mechanical properties. Certainly, one of the most studied allotropic forms of carbon is graphene, which is a single layer of graphite and a semimetal with remarkable electronics properties. However, graphene does not have a bandgap around the Fermi level, which makes it unfeasible for circuit fabrication. In spite of that, as shown in references [4,5], the structures known as hybrid h-BNC can be used in the development of bandgap-engineered electronic devices. For instance, recently an experimental realization has been performed of the hybrid structure of graphene and boron nitrite BC_2N, which were synthesized by chemical vapor deposition of acetonitrile and boron trichloride polycrystalline nickel on quartz substrates [6]. Such experimental results indicate that BC_2N is a p-type semiconductor. It is possible to verify that the atoms of boron and nitrogen in these structures are distributed in an irregular form. On the other hand, it was shown in reference [7] that the maximization of B-N and C-C bonds increases the stability of such structures. Namely, the formation of segregated nanodomains of B and N results in a lower cost in energy. In this form, it is possible to verify that structures with nanodomains of graphene and BN are more stable than those with irregular distributions of C, B and N atoms.

As indicated above, atomic layers of h-BNC material, consisting of irregular nanodomains of BN and graphene have been synthesized [4]. This realization has increased the interest in this subject, and several theoretical studies using first principle calculations have been performed in order to clarify the fundamental properties of such materials [8]. Recently, Liu et al. showed in reference [9] that hybrid monolayers of h-BN and graphene with precisely controlled nanodomain sizes and shapes can be synthesized using lithography patterning and sequential chemical vapour deposition (CVD) growth steps. Then, by means of the appropriate combinations of nanodomains of h-BN and graphene, hybrid devices can be entirely constructed in a monolayer. Nanodomains of h-BN of different shapes and sizes can change the magnetic and electronic properties of graphene [8]. The results showed that these structures have a smaller energy cost when compared to irregular hybrids of $B_xC_yN_z$, and have an intermediate structural stability between h-BN and graphene.

The realization of these hybrids can be used as a method to achieve semiconductor properties in such structures. Another form to tailor such electronic and magnetic properties is by submitting these structures to hydrogen adsorption [10–12], with the advantage of being easier to realize when compared to the formation of vacancies, for example. These studies have shown that the adsorption of hydrogen can give rise to a bandgap opening in the graphene electronic structure and to the emergence of magnetism in these systems. Furthermore,

[a] e-mail: sazevedo@fisica.ufpb.br

$$E_{form} = \frac{E_{Total} - n_{\mathrm{BN}}\mu_{\mathrm{BN}} - n_{\mathrm{CC}}\mu_{\mathrm{CC}} - n_B\mu_B - n_{\mathrm{N}}\mu_{\mathrm{N}} - n_{\mathrm{H}}\mu_{\mathrm{H}}}{n_{atoms}} \quad (1)$$

there is a great interest in the interaction of hydrogen atoms with graphitic compounds in a number of different fields, like hydrogen storage [13,14] and interstellar chemistry [15].

In this work we present first principle calculations to investigate single and double adsorption of hydrogen in a number of different hybrid monolayers, based on the structures studied in reference [8], in order to unveil the changes in the electronic properties of such compounds due to the adsorption of H atoms. It is known that the geometric shape of the h-BN nanodomain in graphene plays an important role on the modulation of the electronic and magnetic properties. Then, for the sake of completeness, we analyze circular-shaped h-BN nanodomains that have the same number of electrons and holes; triangular-shaped structures with nitrogen atoms at the edge, which have an excess of electrons; and triangular-shaped structures with boron atoms at the edge, which exhibit an excess of holes. Therefore, in such cases, we have a complete scenario of electronic configurations to be studied. As we shall see, similar to the introduction of defects in the molecular structure, the adsorption of hydrogen atoms in a hybrid monolayer introduces localized states and induces a change in the energy gap. In addition, such systems can exhibit localized states. In this form, in most of the cases, we may have spin polarization and the appearance of midgap states. We have also found that certain configurations of hybrid monolayers can quench the spin polarization that would be generated by the adsorption of H atoms, and that it depends on which carbon atom adsorbs the hydrogen, as well as the geometry of the nanodomain. The stability of these structures were investigated based on their formation energies. Given the recent progress in synthesizing heterostructures with nanodomains of h-BN and graphene, as well as in the usage of the adsorption of H atoms, we believe that the structures presented here are important candidates to be applied in future experimental implementations in the fields of nanoelectronics and spintronics.

2 Computational method

The calculations were performed by using the density-functional theory (DFT) in the framework of the Generalized Gradient Functional approximations [16], as implemented in the SIESTA code. We make use of the Troullier-Martins pseudopotential [17] and double-basis sets with polarization functions for all the atoms. A separation distance of 20 Å between neighboring systems was used in order to avoid interactions.

For the sake of illustration, Figure 1a shows the geometry of the supercell used in our calculations, which is periodic in the x-y plane. Following the notation of Figure 1, we use the suffix (A_1), for example, when one H atom is adsorbed by the correspondent C atom, and the suffix (A_2A_1) when one H atom is adsorbed at the A_1 C atom and another at the A_2 C atom.

3 Results

3.1 Stability properties

First, we analyze the stability of these structures as a function of the B_xN_y nanodomain and the adsorption of H atoms. The formation energy is calculated by simulating the chemical environment where the structure is synthesized [18]. In this case, it is given by:

see equation (1) above

where n_{BN} and n_{CC} are the numbers of B-N and C-C pairs; n_{B}, n_{N} and n_{H} are the numbers of B, N and H atoms, respectively, and n_{atoms} is the total number of atoms. The parameters μ_{BN} and μ_{CC} are respectively the chemical potentials of the B-N and C-C pairs; and μ_B, μ_{N} and μ_{H} are the chemical potentials of the B, N and H atoms, respectively. The total energy is represented by E_{Total}. The cohesive energy can be obtained with the following equation:

$$E_{co} = \frac{E_{Total} - n_BE_B - n_{\mathrm{N}}E_{\mathrm{N}} - n_{\mathrm{C}}E_{\mathrm{C}} - n_{\mathrm{H}}E_{\mathrm{H}}}{n_{atoms}}. \quad (2)$$

In this case, n_{C} is the number of C atoms, whereas E_{B}, E_{N}, E_{H} and E_{C} are the respective free energies.

As already known, the smaller the formation energy, and the more negative the cohesive energy, the higher the stability and the thermodynamic feasibility of the structure. As we show in Table 1, the formation energy is directly proportional to the size of the B_xN_y nanodomain, since the number of N-C and B-C bonds, which are less stable than C-C and B-N bonds, increases. However, the structures with a triangular-shaped nanodomain have presented small values for the formation energy when compared to the other structures. We believe that this happens because of the geometry of the supercell. Moreover, the adsorption of H atoms increases the formation energy in most of the cases. This happens because of the strain caused by the adsorption. Namely, the partial rehybridization of the C atom where the adsorption takes place from sp^2 to sp^3 means that the adsorption of H atoms is a thermally activated process. However, the discrepancy in the formation energy is small when there is an adsorption; specially in the case of the triangular-shaped nanodomains. As a matter of fact, the adsorption of H atoms at the edges of the B_xN_y nanodomain seems to play a discrete role in the formation energy, especially for the triangular cases. We can also see that the puckering height of the C atom upon adsorption is very similar in most of the configurations. Nevertheless, for the configurations with the triangular-shaped nanodomains,

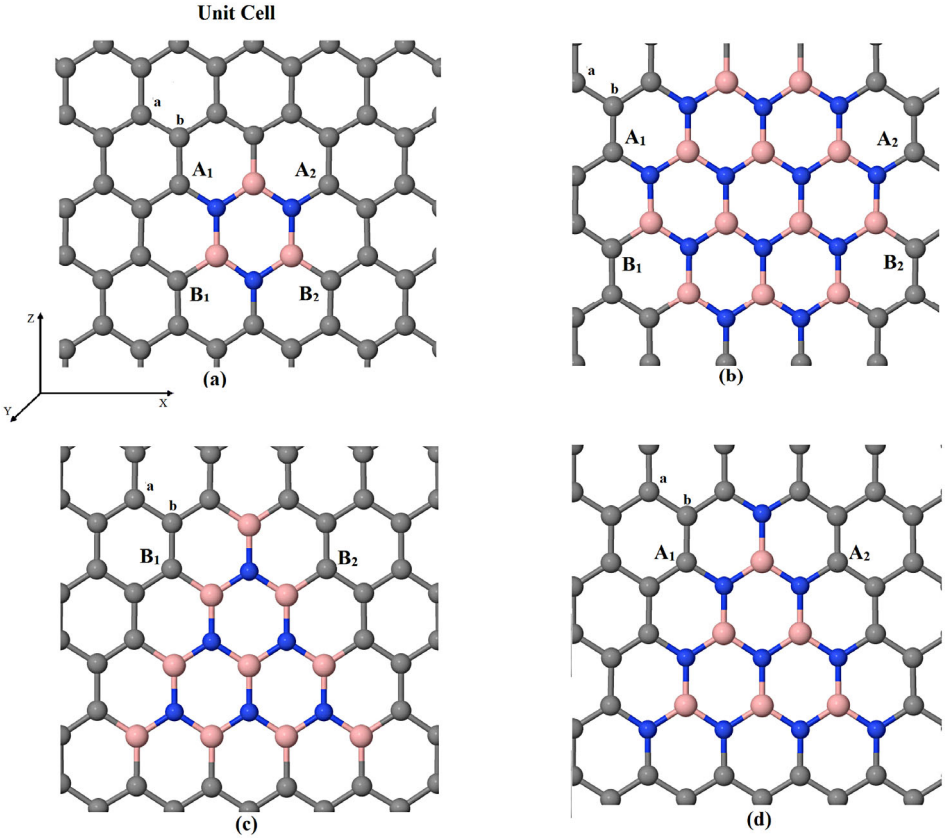

Fig. 1. Representation of all analyzed configurations. The geometry of the unit cell used in the calculations can be seen in (a). In accordance with the notation of reference [8], we adopt the following correspondence: (a) H−B_3N_3, (b) H−$B_{12}N_{12}$, (c) T_b−$B_{10}N_6$ and (d) T_n−B_6N_{10}. The suffixes A_1, A_2, B_1 and B_2 indicate the C atoms at which the adsorpion of the H atom takes place. In this case, the first adsorption occurs either at the A_1 or the B_1 C atom, and the second either at the A_2 or the B_2 C atom. In the nanodomain, B atoms are shown in pink (larger balls) and N atoms in blue (smaller balls). The letters a and b represent the graphene sublattices.

Table 1. Calculated values of the formation energy, the equilibrium distances of the C atom above the surface, the interaction energies of the adsorbed H atom, and the cohesive energies.

Configurations	E_f (eV/atom)	d_{puck} (Å)	E_{int} (eV/atom)	E_{coh} (eV/atom)
H−B_3N_3	0.14	–	–	–7.88
(A_1)H−B_3N_3	0.15	0.35	–1.46	–7.81
(A_2A_1)H−B_3N_3	0.15	0.35	–1.44	–7.74
(B_1)H−B_3N_3	0.15	0.35	–1.48	–7.81
(B_2B_1)H−B_3N_3	0.16	0.35	–1.32	–7.74
(B_2A_1)H−B_3N_3	0.15	0.31	–1.74	–7.75
H−$B_{12}N_{12}$	0.17	–	–	–7.69
(A_1)H−$B_{12}N_{12}$	0.18	0.32	–1.44	–7.62
(A_2A_1)H−$B_{12}N_{12}$	0.18	0.29	–1.47	–7.56
(B_1)H−$B_{12}N_{12}$	0.17	0.28	–1.58	–7.62
(B_2B_1)H−$B_{12}N_{12}$	0.18	0.27	–1.59	–7.56
(B_2A_1)H−$B_{12}N_{12}$	0.17	0.32	–2.01	–7.56
T_b−$B_{10}N_6$	0.13	–	–	–7.78
(B_1)T_b−$B_{10}N_6$	0.13	0.22	–2.54	–7.65
(B_2B_1)T_b−$B_{10}N_6$	0.12	0.23	–2.54	–7.67
T_n−B_6N_{10}	0.14	–	–	–7.69
(A_1)T_n−B_6N_{10}	0.14	0.34	–2.36	–7.63
(A_2A_1)T_n−B_6N_{10}	0.14	0.34	–2.36	–7.58

it depends on which atom the C atom is bound. For the structures with the triangular-shaped nanodomains, when the C atom is bound to a N atom, the puckering height is larger than the one in which the C atom is bound to a B atom. It seems to happen because of the larger electronegativity of the N atoms. The present values are in good agreement with those in references [19,20].

The interaction energy between the adsorbed H atom and the structure is also calculated, and in most of the cases it has values similar to the ones calculated in reference [21] for the adsorption of one H atom in pristine graphene (–1.53 eV). However, we found that when the adsorption occurs first in the B_2 C atom and after in the A_1 C atom, the interaction energy is much larger. This behavior can be explained by means of the valence bond theory, as shown in reference [20]. As we shall show in the next section, most of the configurations will have a spin density upon hydrogen adsorption. If the adsorption occurs at an "**a**" lattice site, the spin density will be localized at "**b**" lattice sites (Fig. 6), so that if the second H atom is adsorbed at a "**b**" lattice site, the unpaired electron that results from this adsorption will readily couple with the unpaired electron of the first adsorption, which is moving through the "**b**" lattice sites. This explains the bigger interaction energies for the (B_2A_1)H$-$B$_{12}$N$_{12}$ and (B_2A_1)H$-$B$_3$N$_3$ configurations. Accordingly, adsorptions of the (B_2A_1) type are more stable than the others described here, which is a result that agrees with those presented in reference [20], as well as with some recent experimental data [22–24]. For the triangular configurations, the interaction energy is much larger than those of the other configurations. Then, we can conclude that the geometry of the defect plays an important role in the adsorption of H atoms and that, for these configurations, the adsorption is more feasible. In addition, we can see that there is a bigger difference between the interaction energies of these configurations, which depends on whether the nanodomain terminates in B or N atoms. Note that when the edge of the nanodomain is composed of B atoms, the interaction energy is more negative than those composed of N atoms. We can assume that it happens because of the redistribution of the charge of the p_z orbitals in the N atoms. Also, the absence of electrons in the p_z orbitals of the B atoms seems to favor the interaction energy in the configurations with nanodomains whose edges are composed of B atoms. We believe that all these structures can be thermodynamically synthesized, as indicated in reference [4].

3.2 Electronic and magnetic properties

To better understand the adsorption of H atoms in the various hybrids, we calculate the band structure, the spin density and the density of states (DOS) of all configurations. First, we focus on the structures with no adsorption; the band structure of these systems can be seen in Figure 2. The band structures of the H$-$B$_3$N$_3$ and H$-$B$_{12}$N$_{12}$ show that these materials are semiconductors due to the insulator nanodomain. Moreover, we can see that the band gap is directly proportional to the size of the insulator

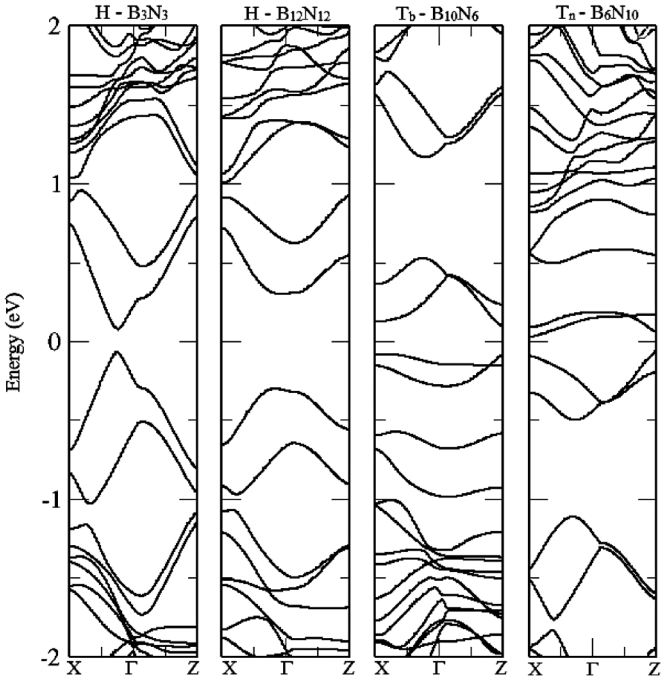

Fig. 2. Band structure of the studied configurations with no adsorption. The energy is scaled with respect to the Fermi energy.

nanodomain; this is because of the larger potential barrier generated by the higher insulator nanodomain. These structures have the same number of electrons of their parental compound, i.e., they are isoelectronic. For this reason, there are no extra charge carriers, and hence, there are no midgap states.

We now analyze the structures with triangular nanodomains. As can be seen from Figure 1, there are two possible configurations for this system: one with the edge terminated in B atoms (T_b-B$_{10}$N$_6$), and another with the edge terminated in N atoms (T_n-B$_6$N$_{10}$). If the system is terminated in B (N), it will have an excess of holes (electrons), that is, these systems may be hole- and electron-doped, respectively. In Figure 2, we find that there are four midgap states for the configurations with triangular nanodomain. This is due to the four holes (electrons) in excess, since there are four extra B (N) atoms in the T_b-B$_{10}$N$_6$ (T_n-B$_6$N$_{10}$) system. Both of these systems are semiconductors, since their midgap states do not cross the Fermi level. These midgap states originate mainly from the orbitals of the C atoms at the edge of the nanodomain, as can be seen from Figure 7. It is also worth noticing that the two systems with triangular shaped nanodomains have an electron-hole symmetry. It can be observed that their band structures are the inverse of each other; this result is in agreement with those of reference [8]. Yet, note that none of the structures without the adsorbed hydrogen possesses magnetic moment. This happens because there is no imbalance in the $\pi - \pi^*$ system, since there is no disappearance of the p_z orbitals.

Now, we analyze the electronic properties of the structures in which the H atoms are adsorbed at the B_1

Table 2. The gap between the occupied and unoccupied bands and the total magnetic moments.

Configurations	Gap (eV)	Magnetic moment (μ_B)
H−B_3N_3	0.14	–
(A_1)H−B_3N_3	0.71	1
(A_2A_1)H−B_3N_3	1.04	2
(B_1)H−B_3N_3	0.7	1
(B_2B_1)H−B_3N_3	1.02	2
(B_2A_1)H−B_3N_3	0.89	–
H−$B_{12}N_{12}$	0.59	–
(A_1)H−$B_{12}N_{12}$	0.71	–
(A_2A_1)H−$B_{12}N_{12}$	1.32	2
(B_1)H−$B_{12}N_{12}$	0.83	1
(B_2B_1)H−$B_{12}N_{12}$	1.26	2
(B_2A_1)H−$B_{12}N_{12}$	1.14	–
T_b−$B_{10}N_6$	0.2	–
(B_1)T_b−$B_{10}N_6$	1.41	0.82
(B_2B_1)T_b−$B_{10}N_6$	1.17	0.64
T_n−B_6N_{10}	0.11	–
(A_1)T_n−B_6N_{10}	1.36	0.7
(A_2A_1)T_n−B_6N_{10}	1.13	–

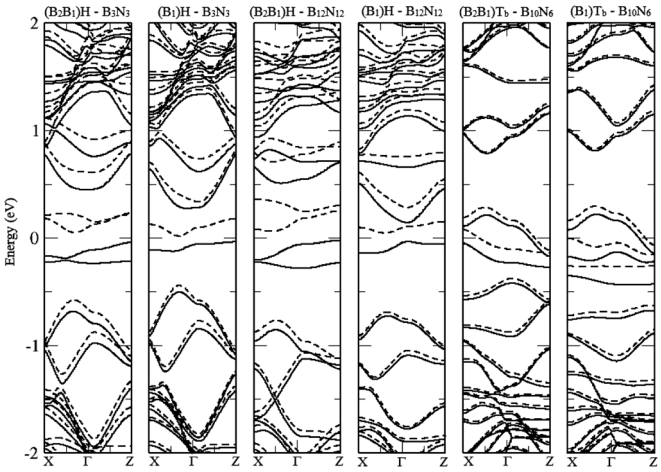

Fig. 3. Band structure of the studied configurations in which the adsorption of a H atom occurs at the B_1 and B_2 C atoms. The solid lines are the spin up states and the dotted lines are the spin down states. The energy is scaled with respect to the Fermi energy.

and B_2 C atoms. The band structures of these systems are shown in Figure 3. The (B_1)H−B_3N_3, (B_2B_1)H−B_3N_3, (B_1)H−$B_{12}N_{12}$ and (B_2B_1)H−$B_{12}N_{12}$ structures can all be classified as semiconductors. In these systems, we can see that for each H atom adsorbed, two midgap polarized spin states take place and, due to the exchange-correlation effects, they are not degenerated. This is a well-known and expected behavior, which is caused by the disappearance of the p_z carbon orbital due to the rehybridization from sp^2 to sp^3 caused by the hydrogen adsorption by the C atom. There is one midgap state for each spin specie; these states have been mapped in our calculations of the spin density and can be seen in Figure 6.

We can see that if the adsorption occurs at an, **a** (or, **b**) lattice site, the spin density will be localized at the corresponding site. This pattern is common to other defects, such as vacancies and edges [25]. The sites with spin density carry most of the magnetic moment shown in Table 2. As explained in reference [20], π conjugated systems have a spin alternation behavior. The π electron system can be understood as a combination of alternating conventional and double bond structures. Specifically, when the H atom is adsorbed, an unpaired electron is left in one of the neighboring C atoms. This electron can, in turn, move through each of the C atoms belonging to this sublattice, due to the resonant behavior of the system (Fig. 6). It was shown in reference [21] that a band gap of 1.25 eV is open upon H adsorption in pristine graphene. Furthermore, it was demonstrated that this band gap is caused by the appearance of the H^+ ion. Our results for the band gap (Tab. 2) shows that the gap opening caused by the H^+ ion is smaller when there is a B_xN_y with $x = y$ nanodomain. It seems that the nanodomain causes the ion to have a weaker effect on the band structure of the system; except for the systems with triangular-shaped nanodomains.

Figure 3 shows that the configurations with triangular-shaped nanodomain have a different behavior upon hydrogen adsorption, when compared to the isoelectronic nanodomains. First, since their midgap states cross the Fermi level, they are both metallic. Second, the configuration (B_1)T_b−$B_{10}N_6$ has a magnetic moment of $0.82\mu_B$ (Tab. 2), and three pairs of spin polarized midgap states due to the adsorption of a H atom, although there is only one hydrogen adsorbed. In turn, Figure 6 shows that there is no spin density in the vicinity of the hydrogen atom, which means that its electron is not left unpaired, but instead takes part of the electron-hole system of the compound. The same behavior seems to happen in the (B_2B_1)T_b−$B_{10}N_6$ configuration, except that in this case there are two electrons from the adsorbed hydrogen atoms. This system has a slightly smaller magnetic moment of $0.64\mu_B$, as well as a smaller bandgap (Tab. 2). We believe that, upon the adsorption of the second hydrogen, the band gap in systems with triangular-shaped nanodomain is smaller because of the smaller contribution of the H^+ ion, since in this case the electrons of the H atoms are part of the $\pi - \pi^*$ band system. In addition, Figure 6 shows that for all the configurations with triangular-shaped nanodomains, the density of spins is concentrated in the same sublattice in which the H atom is adsorbed. This indicates that the holes move from the B atoms to the first neighboring C atoms, and then to the C atoms in the same sublattice.

Figure 4 shows the band structures of the configurations in which one H atom is adsorbed at the B_2 and A_1 C atoms. These configurations do not have any magnetization; this can be explained by the Valence Bond theory [20], as mentioned earlier. Since the H atoms are adsorbed by the C atoms from different sublattices, it renders an electron from the H atom of the second adsorption pair together with an electron from the H atom of the first adsorption such that there is no unpaired electron, and, therefore, we have no magnetic moment. This configuration is called AB dimer. As expected, the band gap

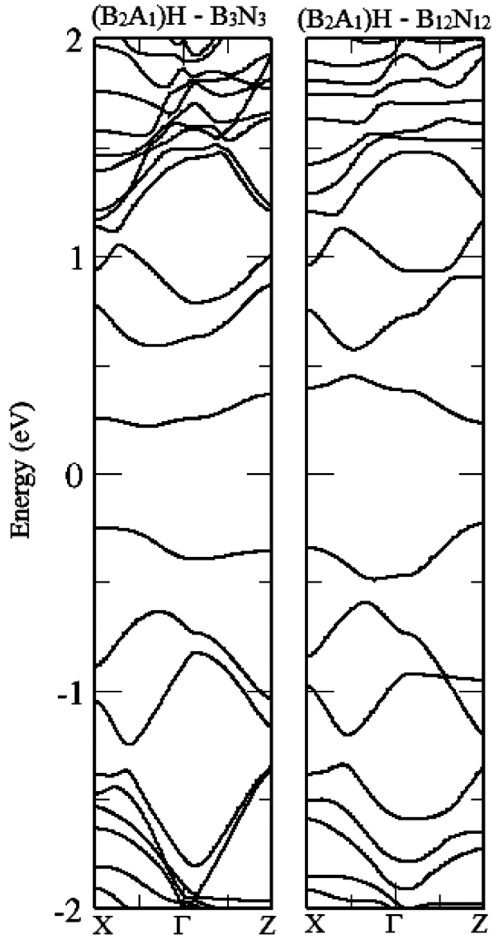

Fig. 4. Band structure of the studied configurations in which the H adsorption occurs in the B_2A_1 C atoms. The energy is scaled with respect to the Fermi energy.

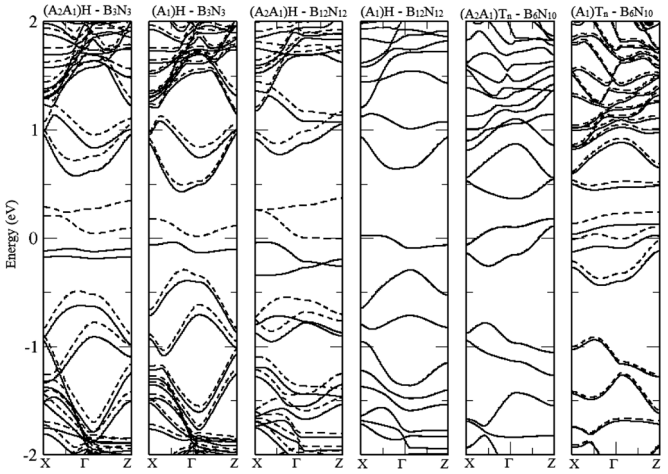

Fig. 5. Band structure of the studied configurations in which the adsorption of the H atom occurs at the A_2 and A_1 C atoms at the same time. The solid lines are the spin up states and the dotted lines are the spin down states. The energy is scaled with respect to the Fermi energy.

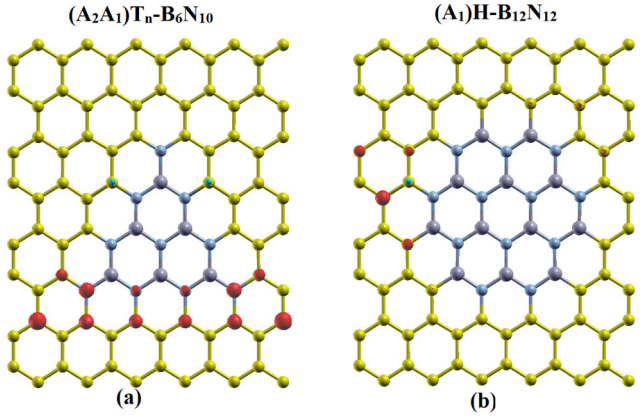

Fig. 6. Density of spin for the configurations in which the adsorption of the H atom occurs in the compounds with triangular shaped nanodomains. The C, N, B and H atoms are yellow, blue, purple and green respectively.

is directly proportional to the size of the nanodomains, as can be seen in Table 2. Also, we can see that the midgap states generated by the H atoms adsorbed are degenerated, since the electrons from the H atoms are paired.

We now focus on the systems in which the H atom is adsorbed in the A_1 and A_2 C atoms. Figure 5 shows the band structures of these configurations for the first three bands. For the configurations (A_2A_1)H$-$B$_3$N$_3$, (A_1)H$-$B$_3$N$_3$ and (A_2A_1)H$-$B$_{12}$N$_{12}$, we have the usual behavior upon hydrogen adsorption: all the structures are semiconductors, the generation of a pair of spin polarized states per H atom adsorbed, and the magnetization of the system. However, the configuration (A_1)H$-$B$_{12}$N$_{12}$ is metallic and does not have magnetic moment; there is one midgap state that crosses the Fermi Level. The density of states shows that the midgap state is mainly a contribution of the C atoms, which are also expected to have a density of spin as shown in Figure 7. It seems that the exchange-correlation energy was not capable of lifting the degeneracy of the midgap state. For the case of the $(A_1)T_n-$B$_6$N$_{10}$ configuration, we have a metallic compound with three pairs of spin polarized midgap states. We believe that the electron from the adsorbed H atom pairs with one of the four electrons in excess in the structure, and partially lifts the degeneracy of the remaining three electrons, since the magnetic moment is not an integer (Tab. 2).

Similar to the case of the $(B_1)T_b-$B$_{10}$N$_6$ configuration, there is no spin density in the vicinity of the H atom, as shown in Figure 6. For this case, however, there is a more significant contribution to the spin density from the N atoms at the edge of the triangular nanodomain opposite to the H atom. The configuration $(A_2A_1)T_n-$B$_6$N$_{10}$ shows a different behavior. It seems that both electrons of the two adsorbed H atoms paired with two of the four electrons in excess. However, there is no increase in degeneracy, and the magnetic moment is null. There are two degenerated midgap states that correspond to the two remaining electrons in excess from the N atoms. As can be seen from Figure 7a, the density of states is highly concentrated in the lower edge of the triangle with a big

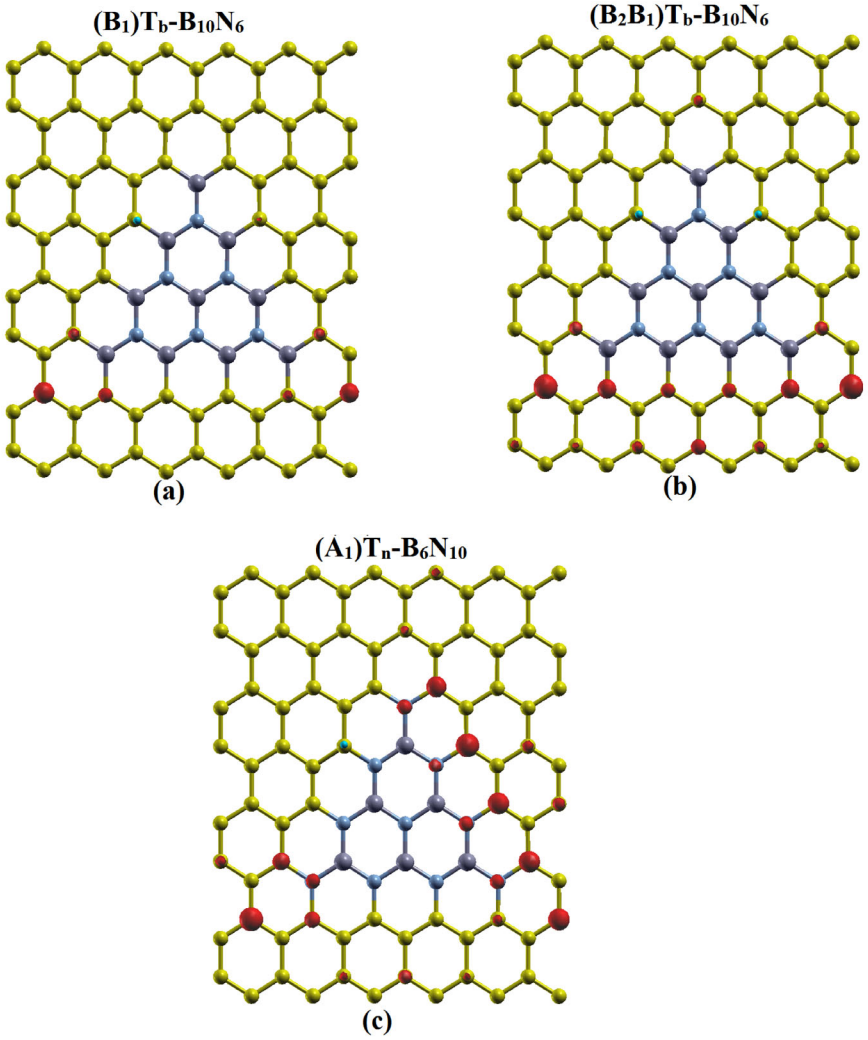

Fig. 7. Density of states for the configurations in which the spin is quenched. The C, N, B and H atoms are yellow, blue, purple and green respectively.

contribution of the N atoms, due to the redistribution of charges in the p_z orbitals. If we compare Figures 6c and 7a, it seems that the adsorbed H atom at the right side of the triangle localizes the states and, therefore, quenches the spin by localizing the states at both sides of the triangle. It seems that the N atoms which are bonded to the C atoms where the hydrogen is adsorbed in the configurations $(A_1)\mathrm{H}{-}\mathrm{B}_{12}\mathrm{N}_{12}$ and $(A_2A_1)T_n{-}\mathrm{B}_6\mathrm{N}_{10}$ play an important role in quenching the spin density of the structure. This behavior does not happen when there are B atoms in place of the N atoms. We can say that the redistribution of charge in the p_z orbitals of the N atoms have the potential to quench the magnetic moment on this type of material.

4 Conclusion

In conclusion, by using first-principles calculations, we have investigated the stability, the electronic and magnetic properties of various hybrid structures with h-BN nanodomains of different geometries. Furthermore, we have investigated the effects of the adsorption of one and two hydrogen atoms at the edges of the nanodomains of such compounds. We have found that the configurations with triangular-shaped nandomains and the $\mathrm{H}{-}\mathrm{B}_3\mathrm{N}_3$ configuration are the most stable. Nevertheless, upon hydrogen adsorption, the former ones were shown to be more stable, although the adsorption of hydrogen does not seem to exert a decisive influence on the formation energy of the configurations in general. We also conclude that the geometry of the nanodomain plays an important role in the value of the interaction energy between the adsorbed hydrogen atom and the structure. We have also shown that the adsorption of H atoms generates an integer magnetic moment in most of the configurations and a non-integer magnetic moment in the configurations with triangular-shaped nanodomains. Figure 6 showed that the pattern of the distribution of the spin density charge follows the expected pattern for a vacancy or the adsorption by a scattering

center, except for the structures with triangular-shaped nanodomains, in which the H atom seems to localize the states around it. It is worth noticing that there is no magnetization for the configurations in which the H atoms are adsorbed at the B_2 and A_1 C atoms. This fact can be explained by the valence bond theory [20]. Moreover, we showed that the configurations $(A_1)\mathrm{H}{-}\mathrm{B}_{12}\mathrm{N}_{12}$ and $(A_2A_1)T_n{-}\mathrm{B}_6\mathrm{N}_{10}$ are metallic and do not have magnetic moment, even when the adsorption of hydrogen takes place. In general terms, we see that both the atoms at which the H atom is adsorbed and the geometry of the nanodomain played a decisive role in the electronic and magnetic properties of the studied compounds.

Author contribution statement

T.S.S. and S.A. contributed to the conception and development of the ideas. T.S.S. performed the calculations. T.S.S., S.A. and B.L.B. contributed to the writing of the manuscript and discussion of the results.

T.S.S. and S.A. acknowledge the support from the Brazilian funding agencies CNPq, CAPES/NANOBIOTEC, and INCT – Nanomateriais de Carbono.

References

1. A.H. Castro Neto, F. Guinea, N.M.R. Peres, K.S. Novoselov, A.K. Geim, Rev. Mod. Phys. **81**, 109 (2009)
2. A.K. Geim, K.S. Novoselov, Nat. Mater. **6**, 183 (2007)
3. M.I. Katsnelson, Mater. Today **10**, 20 (2007)
4. L. Ci, L. Song, C. Jin, D. Jariwala, D. Wu, Y. Li, A. Srivastava, Z.F. Wang, K. Storr, L. Balicas, F. Liu, P.M. Ajayan, Nat. Mater. **9**, 430 (2010)
5. P.P. Shinde, V. Kumar, Phys. Rev. B **84**, 125401 (2011)
6. M.O. Watanabe, S. Itoh, K. Mizushima, T. Sasaki, J. Appl. Phys. **78**, 4 (1995)
7. S. Azevedo, J.R. Kaschny, C.M.C. de Castilho, F. de Brito Mota, Nanotechnology **18**, 495707 (2007)
8. A.K. Manna, S.K. Pati, J. Phys. Chem. C **115**, 10842 (2011)
9. Z. Liu, L. Ma, G. Shi, W. Zhou, Y. Gong, S. Lei, X. Yang, J. Zhang, J. Yu, K.P. Hackenberg, A. Babakhani, J.-C. Idrobo, R. Vajtai, J. Lou, P.M. Ajayan, Nat. Nanotechnol. **8**, 119 (2013)
10. R. Balog, B. Jørgensen, L. Nilsson, M. Andersen, E. Rienks, M. Bianchi, M. Fanetti, E. Lægsgaard, A. Baraldi, S. Lizzit, Z. Sljivancanin, F. Besenbacher, B. Hammer, T.G. Pedersen, P. Hofmann, L. Hornekær, Nat. Mater. **9**, 315 (2010)
11. M. Mirzadeh, M. Farjam, J. Phys.: Condens. Matter **24**, 235304 (2012)
12. H.G. Herrero, J.M. Gómez-Rodríguez, P. Mallet, M. Moaied, J.J. Palacios, C. Salgado, M.M. Ugeda, J.-Y. Veuillen, F. Yndurain, I. Brihuega, Science **352**, 437 (2016)
13. S. Yadav, Z. Zhu, C.V. Singh, Int. J. Hydrogen **39**, 4981 (2014)
14. L. Wang, N.R. Stuckert, R.T. Yang, AIChE J. **57**, 2902 (2011)
15. L. Jeloaicaa, V. Sidis, Chem. Phys. Lett. **300**, 157 (1999)
16. J.P. Perdew, K. Burke, M. Ernzerhof, Phys. Rev. Lett. **77**, 3865 (1996)
17. N. Troullier, J.L. Martins, Phys. Rev. B **43**, 1993 (1991)
18. S. Azevedo, Phys. Lett. A **351**, 109 (2006)
19. X. Sha, B. Jackson, Surf. Sci. **496**, 318 (2002)
20. S. Casolo, O.M. Løvvik, R. Martinazzo, G. Franco Tantardini, J. Chem. Phys. **130**, 054704 (2009)
21. E.J. Duplock, M. Scheffler, P.J.D. Lindan, Phys. Rev. Lett. **92**, 225502 (2004)
22. A. Andree, M. Le Lay, T. Zecho, J. Küppers, Chem. Phys. Lett. **425**, 99 (2006)
23. L. Hornekaer, Z. Sljivancanin, W. Xu, R. Otero, E. Rauls, I. Stensgaard, E. Laegsgaard, B. Hammer, F. Besenbacher, Phys. Rev. Lett. **96**, 156104 (2006)
24. L. Hornekaer, E. Rauls, W. Xu, Z. Sljivancanin, R. Otero, I. Stensgaard, E. Laegsgaard, B. Hammer, F. Besenbacher, Phys. Rev. Lett. **97**, 186102 (2006)
25. O.V. Yazyev, Rep. Prog. Phys. **73**, 056501 (2010)